JOURNAL OF MATERIALS SCIENCE 21 (1986) 3823–3828

A practical approach to the determination of the crystallography of grain boundaries

VALERIE RANDLE, BRIAN RALPH
Department of Metallurgy and Materials Science, University College, Cardiff, UK

Methods available for determining the crystallography of grain boundaries are surveyed. It is suggested that the reason why relatively few studies of the crystallography of large numbers of boundaries have been made is the intensity of labour involved in the data analysis. A scheme is described which allows a large sample population of grain boundaries to be handled with maximum efficiency, whilst maintaining high precision in the parameters which describe the boundary. It also permits a comparison of these parameters with those which describe special cases (e.g. high-density coincidence site lattice, etc). The method involves a combination of stereographic manipulation and matrix algebra.

1. Introduction

In recent years, models of grain-boundary structure have been considerably extended. The coincidence site lattice (CSL) representation has tended to predominate as the basis of the more significant models of grain-boundary geometry (e.g. [1–4]). CSL boundaries have special properties and are often associated with low energies [5]. An axis of misorientation/angle of misorientation pair is commonly used to describe the relationship between two grains; the axis of misorientation, l, is a direction which is common to both grains about which the first grain must be rotated by the angle of misorientation, θ, in order to achieve the orientation of the second.

The collection and analysis of experimental misorientation data has not received as much attention as has the development of theoretical boundary models. Most of the experimental support for these models arises from studies on especially prepared and oriented bicrystals [6]. The absence of data which relate to more common materials in their polycrystalline form reflects the labour-intensity of producing accurate crystallographic results in these cases.

This paper describes a method whereby diffraction data from large sample populations of boundaries may be collected efficiently and analysed to supply both an axis/angle pair and a correlation with a CSL representation of each boundary.

2. Experimental procedure

A commercially produced alloy, Nimonic PE16 (Henry Wiggin & Co., Hereford, UK) was investigated and diffraction data taken from about one hundred boundaries, as part of an ongoing investigation into grain-boundary structure as a function of ageing parameters for this alloy. [7]. Experimental work was carried out on a Philips 400T transmission electron microscope. Results were processed using a Tektronix 4051 microcomputer.

3. Methods available for the analysis of grain-boundary geometry

Two basic approaches exist for the determination of axis/angle pairs from diffraction patterns. Firstly, an analytical approach such as that due to Young *et al.* [8] characterizes the misorientation by a 3×3 matrix whose columns represent the direction cosines of Grain 1 referred to Grain 2. The simplest case of a twin boundary in the cubic system is used here as an example. For this case, one in three atomic sites are common to both crystals and therefore it is referred to as a $\Sigma = 3$ boundary*. Fig. 1 shows how Grain 2 may be rotated into Grain 1 through an angle of 60° about the [1 1 1] misorientation axis, which, by definition, is common to both crystals. The matrix which describes this rotation is given by

$$R = \frac{1}{3}\begin{pmatrix} 2 & \bar{1} & 2 \\ 2 & 2 & \bar{1} \\ \bar{1} & 2 & 2 \end{pmatrix} \quad (1)$$

The second approach which can be used to yield misorientation data relies on standard stereographic procedures. Of the methods using stereographic manipulation perhaps the best known is that due to Goux [9]. Two pairs of diffraction patterns from each side of the boundary are required. This method is based on the fact that the pattern zone axes in both grains (A1 and A2) must be parallel, from which it follows that the axis of misorientation lies on a zone which is equidistant from A1 and A2. In turn this zone is represented on the stereogram as the great circle which bisects the great circle through A1 and A2.

If a similar treatment is applied to the second pair of zone axes B1 and B2, the axis of misorientation, l, is given by the intersection of the zones which bisect A1, A2 and B1, B2, respectively. The angle of rotation θ is found from projecting A1 and A2 on to the zone which contains the pole of l (Fig. 2). The angle between A′1 and A′2 defines θ.

*In the CSL model Σ is merely defined as the reciprocal of the density of common sites.

0022–2461/86 $03.00 + .12

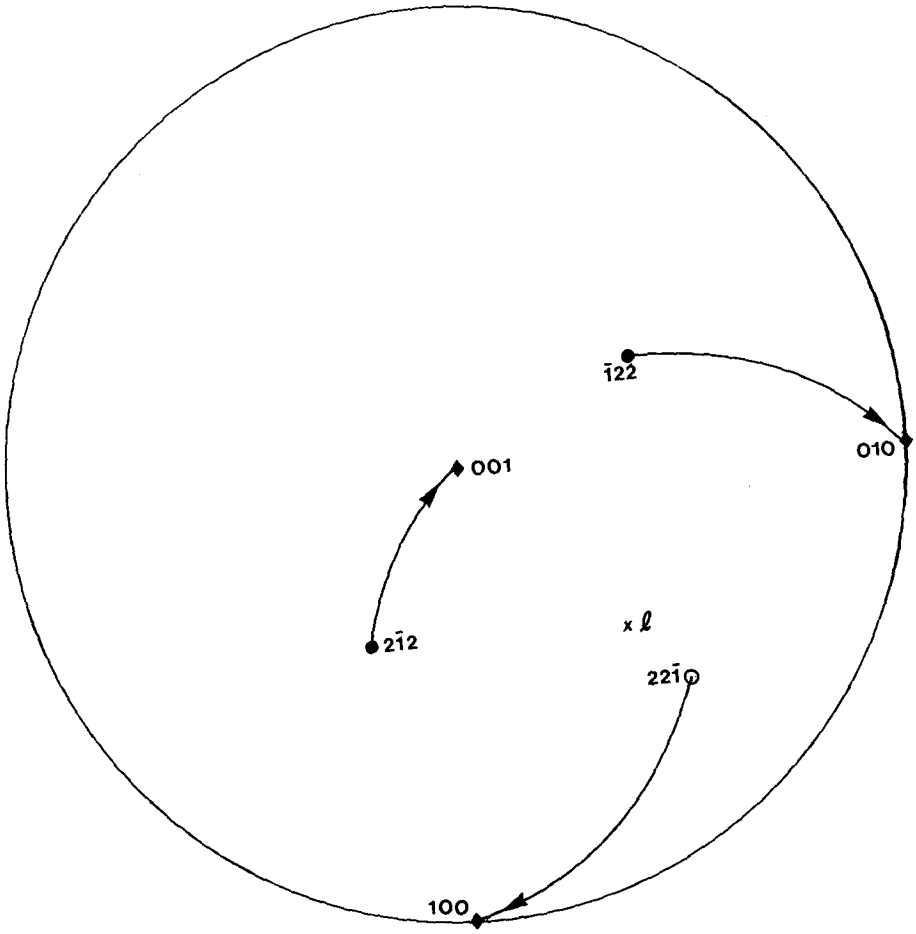

Figure 1 Stereographic representation of a twin-related bicrystal. A clockwise rotation of 60° about the 1 1 1 axis – common to both crystals – rotates the $2\bar{1}2$, $\bar{1}22$ and $22\bar{1}$ directions in Crystal 2 on to the crystal axes of Crystal 1. (◆) Grain 1, (●) Grain 2.

A less widely known method is that due to Ralph [10]. It requires the knowledge of three pairs of non-tautozonal directions or plane normals which have the same indices in both crystals. Usually, the crystal axes are selected, and these are plotted in pairs on the stereogram $(h\,k\,l)_1$ and $(h\,k\,l)_2$, etc.

When both grains are rotated on to a common reference frame (e.g. the edges of the photographic

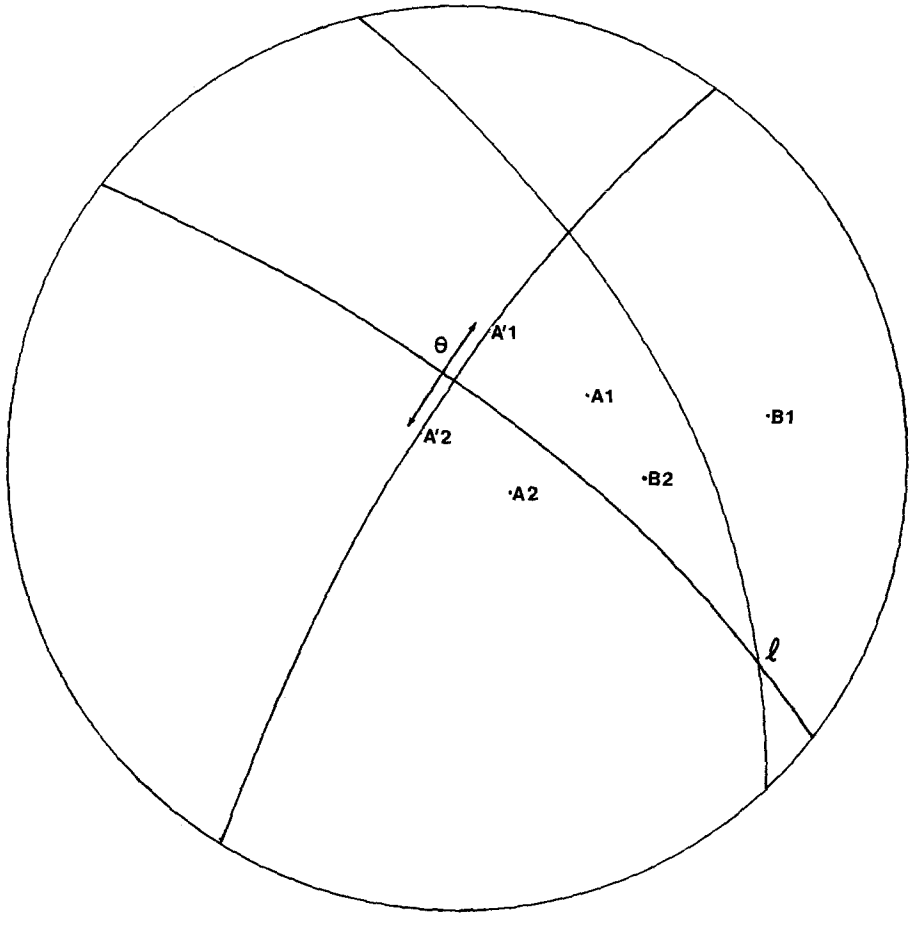

Figure 2 Determination of the misorientation parameters for Boundary 4 using the Goux stereographic method. A1, A2, and B1, B2 are two pairs of parallel directions in Grains 1 and 2. The axis of misorientation, l, is defined by the intersection of great circles which bisect A1, A2 and B1, B2. The angle of misorientation, θ, is given by the angle between A'1 and A'2 where A'1 and A'2 are the projections of A1 and A2 into the invariant plane, i.e. the great circle of which l is the pole.

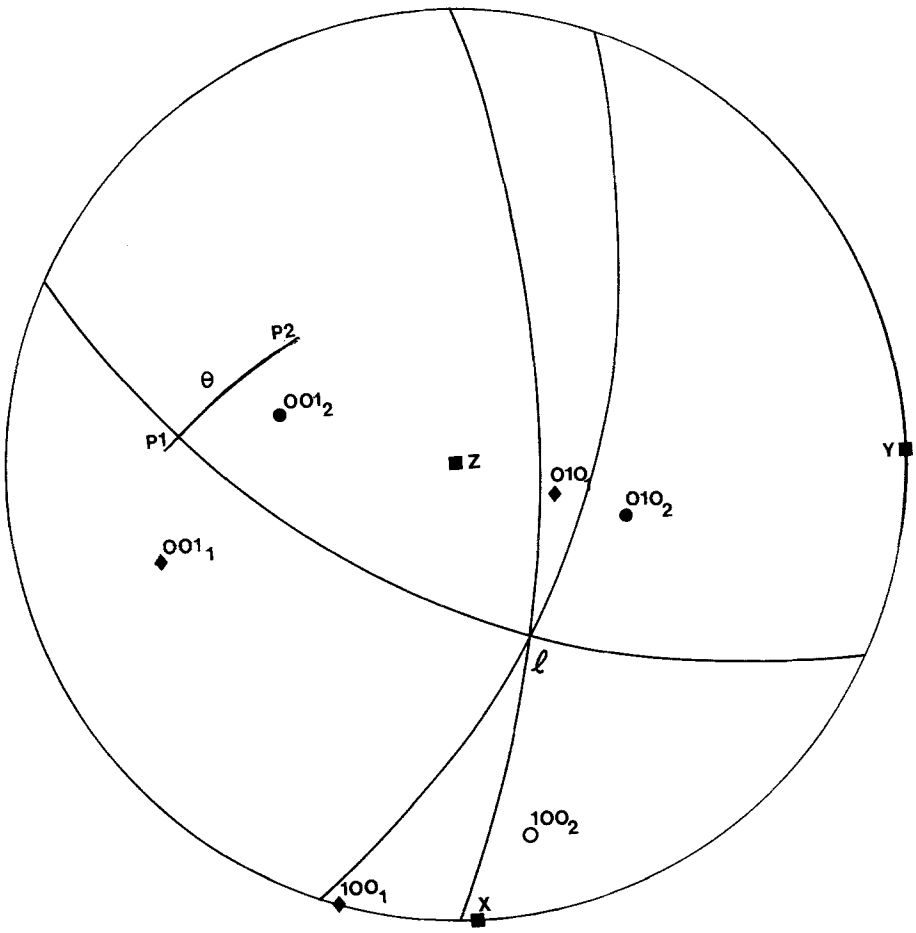

Figure 3 Determination of the misorientation parameters for Boundary 3 using the Ralph stereographic method. The crystal axes of (◆) Grain 1 and (●) Grain 2 have been rotated on to a common reference frame XYZ. P1 and P2 are the poles of great circles containing l, $0\,1\,0_1$ and l, $0\,1\,0_2$, respectively, where the subscripts refer to Grains 1 and 2. The axis of misorientation, l, is defined by the intersection of great circles which bisect $0\,0\,1_1$ and $0\,0\,1_2$, $0\,1\,0_1$ and $0\,1\,0_2$, $1\,0\,0_1$ and $1\,0\,0_2$. The angle of misorientation, θ, is given by the angle between P1 and P2.

plate) the axis of misorientation, l, lies on a zone which is equidistant from each pair of directions/plane normals. Since there are three such pairs, l is defined accurately as the intersection of the great circles which bisect the pairs $(h\,k\,l)_1$ to $(h\,k\,l)_2$, etc. The angle between the poles P_1 and P_2 of great circles containing l, $(h\,k\,l)_1$ and l, $(h\,k\,l)_2$, respectively, gives θ (Fig. 3).

4. Procedure for geometrical analysis of grain boundaries

4.1. Acquisition of diffraction data

The axis/angle pair determination depends firstly upon the generation of precise diffraction data in order to define accurately the orientation from both sides of a grain boundary. In the transmission electron microscope (TEM) this is most easily achieved by use of microdiffraction with a convergent probe. Several reviews of microdiffraction have been published (e.g. [11, 12]). Essentially, the convergent probe relaxes the conditions necessary for the excitation of Kikuchi lines as compared to their generation by conventional selected-area diffraction. This imposes far less restrictions upon the thickness of crystal from which accurate diffraction data may be collected. Fig. 4 shows two examples of pattern pairs, which have been used to analyse Boundaries 3 and 4 in Table I. The first pair (Figs 4a and b) arise from near the foil edge where the crystal is thin enough for discrete diffraction maxima (discs) to be visible. Figs 4c and d have been taken from thicker regions of crystal, and now the Kikuchi line visibility predominates over that of the diffraction discs.

There are other advantages associated with the use of microdiffraction for this work. The use of a well-aligned microscope permits calibration of the reciprocal lattice section for a particular camera length. It then becomes a simple matter to transfer accurate beam directions directly to the stereogram. In practice it was found helpful to tilt to an on-zone pattern (e.g. Fig. 4c) or to the situation where a major Kikuchi line pair is excited (e.g. Fig. 4b) in one grain. Furthermore, if the microscope is operated using a low camera length, enough of the reciprocal lattice section is visible on the plate to be able to determine the absolute beam direction. By contrast, in selected-area diffraction a 180° ambiguity exists so that it is necessary to take pairs of diffraction patterns from each grain before and after a tilt of the specimen. This establishes whether the beam direction for each crystal lies in a right-hand or left-hand unit stereographic triangle [13]. This difficulty does not arise in microdiffraction patterns and so, in general, a single pair of patterns across the boundary suffices. A camera of nominal length 210 mm was adopted for the investigation reported here.

4.2. Processing of the diffraction data

The procedure for the determination of axis/angle pairs by the Ralph method was outlined earlier (Section 3). This method has been used during the present study rather than the Goux or matrix algebra methods, because it contains a built-in check of the accuracy. Fig. 3 illustrates the application of the Ralph method. If the data have been plotted accurately and no errors have been made, the misorientation axis will be represented as the point of

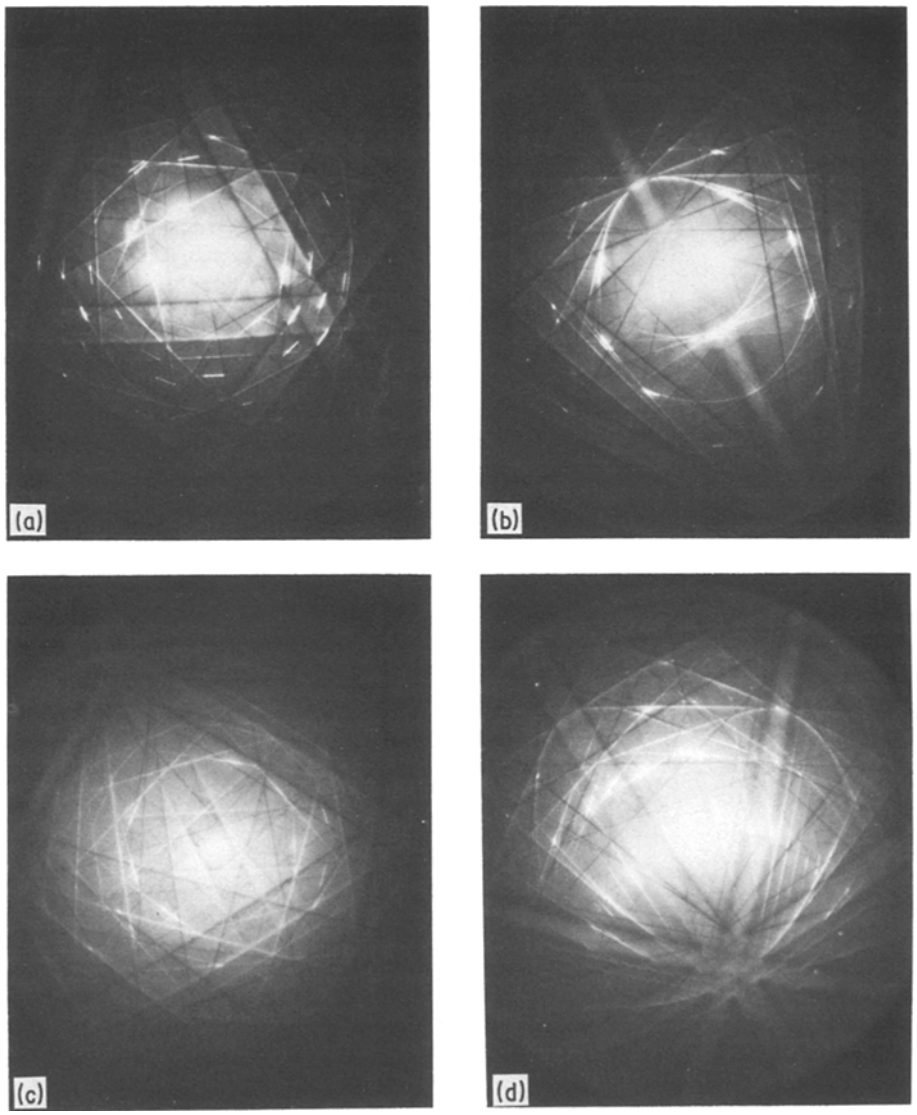

Figure 4 (a, b) Microdiffraction patterns from either side of Boundary 4, where the crystal is relatively thin, therefore discrete diffraction discs are visible. (c, d) Microdiffraction patterns from either side of Boundary 3, where the crystal is relatively thick, therefore Kikuchi line visibility is enhanced in comparison to (a) and (b).

intersection of three great circles. These great circles represent the loci of poles which make equal angles with equivalent poles, $(h\,k\,l)_1$ and $(h\,k\,l)_2$, in the two grains. Any inaccuracy will result in a triangle of uncertainty for l. During this study, which involves the analysis of about 100 boundaries [7], the maximum angular size of this triangle of uncertainty was 1° while for 74% of the cases analysed the triangle was too small to measure. Clearly the accuracy of this analysis also depends on the ability to establish the reference frame system precisely. Here the likely difficulty arises from any twisting of the photographic plate in the camera system of the microscope. In practice in the studies reported here, this did not seem to give rise to any measurable inaccuracy.

A few boundaries were analysed by the Goux method for comparison with the Ralph method. The misorientation relationships obtained for both are listed in Table I.

4.3. Comparisons of the experimental misorientation data with those predicted by CSL theory

The axis/angle pair representation of grain-boundary misorientation is only meaningful if it can then be used to determine the "class" of a boundary, e.g. random, low-angle or special (near a CSL orientation) (e.g. [3]). Therefore the next stage in the grain-boundary analysis scheme reported here was the design of a computer program which outputs the

TABLE I Illustration of the use of the Ralph and Goux methods for the determination of grain boundary parameters

Boundary No.	Axis/angle pair		CSL description of boundary	CSL limit	Actual duration of boundary from exact CSL
	Goux method	Ralph method			
1	0.927, 0.342, 0.105/58°	0.900, 0.342, 0.301/60°	Σ 9 = 3 1 1/67.11°	5.0°	5.4°
		1.00 , 0.761, 0.049/43.8°	Σ 9 = 1 1 0/38.94°	5.0°	5.9°
2	0.866, 0.367, 0.309/22°	0.866, 0.399, 0.309/35.5°	Σ3 3 = 3 1 1/33.60°	2.6°	2.1°
3	0.883, 0.375, 0.035/16°	0.980, 0.130, 0.105/22.3°	Σ1 3 = 1 0 0/22.62°	4.2°	3.1°
4	0.898, 0.357, 0.191/30°	0.823, 0.545, 0.191/38°	Random	–	–
5		0.707, 0.574, 0.431/18°	Σ3 1 = 1 1 1/17.9°	2.7°	2.7°

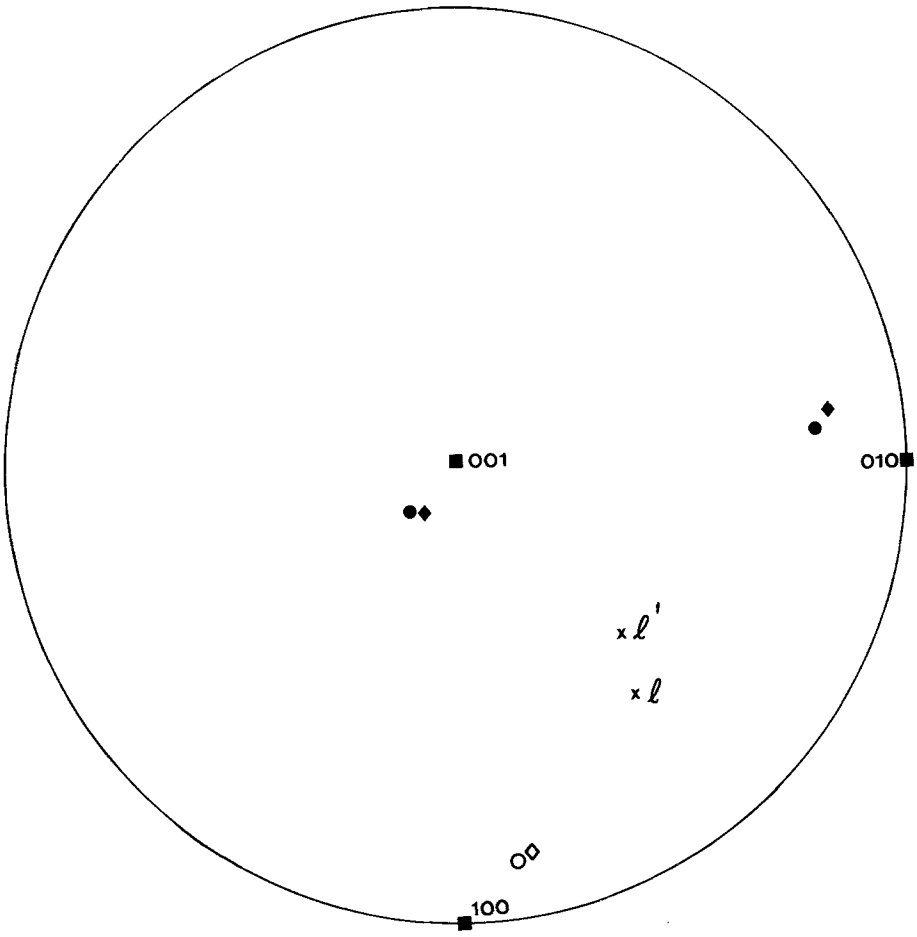

Figure 5 Stereographic representation of (●) Boundary 5, 0.707, 0.574, 0.431/18° and (◆) a $\Sigma = 31$ CSL, 1 1 1/17.9° with Grain 2 referred to the crystal axes of Grain 1. The deviation between the experimental and CSL boundary is 2 to 3°, despite the fact that the angular difference between their respective axes of misorientation (l and l') is 11.2°.

deviation of a particular boundary from the nearest CSL and assesses the significance of this deviation. The steps involved in compiling this program are outlined below.

The first part of the program implements Ranganathan's function [1] in order to generate all possible values of θ and Σ for a particular l (with indices HKL), up to operator-specified limits. In the cubic system values for θ and Σ are derived thus:

$$\Sigma = x^2 + (H^2 + K^2 + L^2)y^2 \quad (2)$$

$$\theta = 2 \tan^{-1} \frac{y}{x(H^2 + K^2 + L^2)^{1/2}} \quad (3)$$

where x and y can have values $\geqslant 0$.

It is necessary to make a subjective choice for the nearest CSL to an experimental boundary. Unless HKL is near a high-symmetry axis (e.g. Boundaries 1, 2 and 3 in Table I which are obviously near 3 1 1, 3 1 1 and 1 0 0, respectively) two or more potential CSL solutions should be selected. The correct choice (i.e. the closest "fit" to the experimental boundary) is apparent after running the program using each potential CSL in turn. This is illustrated with reference to Boundary 5 in Table I. It is not obvious from inspection that the axis/angle pair 0.707, 0.574, 0.431/18° can be described as the 1 1 1/17.9° solution of a $\Sigma = 31$ boundary, since the misorientation axis is 11.2° removed from 1 1 1. Fig. 5 shows a stereographic representation of both the experimental and the CSL case, which clearly demonstrates that the boundary is in fact close to a $\Sigma = 31$ CSL.

From consideration of how closely secondary intrinsic grain-boundary dislocation cores in a CSL boundary may approach before overlap begins, the angular limit for a CSL description is generally assumed to be [14, 15]

$$V = V_0 \Sigma^{-1/2} \quad (4)$$

where V is the CSL angular limit and V_0 is the angular limit for the low-angle boundary description. It is intended as a guide only, particularly since V_0 is approximate. Boundary 1 in Table I has been analysed using a second symmetry-related variation of its axis/angle pair, which can be described by two solutions for a $\Sigma = 9$ CSL. The computations for each case differ by 0.5° (final column of Table I), which highlights the approximate nature of the CSL limit criterion.

The most efficient way of comparing an experimental determination of boundary misorientation with the predicted important CSL descriptions is to use a rotation matrix description for both. Such a rotation matrix, whose columns are the direction cosines of Grain 1 referred to the crystal axes of Grain 2, can be formulated by application of spherical trigonometry (e.g. [16, 17]).

The matrix elements for the cubic case are given by

$$R_{11} = P_1^2 (1 - \cos\theta) + \cos\theta$$

$$R_{12} = P_1 P_2 (1 - \cos\theta) - P_3 \sin\theta$$

$$R_{13} = P_1 P_3 (1 - \cos\theta) + P_2 \sin\theta$$

$$R_{21} = P_2 P_1 (1 - \cos\theta) + P_3 \sin\theta$$

$$R_{22} = P_2^2 (1 - \cos\theta) + \cos\theta$$

$$
\begin{aligned}
R_{23} &= P_2P_3(1 - \cos\theta) - P_1 \sin\theta \\
R_{31} &= P_3P_1(1 - \cos\theta) - P_2 \sin\theta \\
R_{32} &= P_3P_2(1 - \cos\theta) + P_1 \sin\theta \\
R_{33} &= P_3^2(1 - \cos\theta) + \cos\theta
\end{aligned} \tag{5}
$$

where P_1, P_2, P_3 are vector components of the rotation axis $\boldsymbol{P}$, which is defined as a unit vector.

For a cubic crystal, there are 24 equivalent symmetry-related solutions for a misorientation relationship. An example of a complete list of all 24 variations, plus each symmetry operation, has been published by Pumphrey and Bowkett [18] for a $\Sigma = 21$, 112/44.42° boundary and by Randle and Ralph [19] for a $\Sigma = 5$ boundary. By convention, the axis/angle of misorientation is usually but not invariably adopted. It is therefore necessary to generate matrices of the complete set of 24 axis/angle pairs in order to choose that solution whose leading diagonal contains the three largest matrix elements, since the angle and axis of misorientation can be obtained from the transformation matrix thus [20]:

$$
\theta = \cos^{-1}(R_{11} + R_{22} + R_{33} - 1)/2 \tag{6}
$$

$$
H:K:L = R_{21} - R_{12}:R_{13} - R_{31}:R_{32} - R_{23} \tag{7}
$$

The second part of the computer program is designed to premultiply the transformation matrix by each orthogonal matrix which represents a symmetry operation in turn [16]. When the axis/angle pair is in its lowest-angle form, clearly any low-angle boundary situations are immediately identified.

Once matrices have been formulated for the experimental and CSL case, a direct comparison can be made by calculation of the angular difference between the column of the CSL matrix with the respective columns of the experimental matrix. With reference to Boundary 5, which is illustrated in Fig. 5, the appropriate matrices are

$$
\boldsymbol{R}_{\text{expt.}} = \begin{pmatrix} 0.975 & -0.113 & 0.191 \\ 0.152 & 0.967 & -0.205 \\ -0.161 & 0.229 & 0.960 \end{pmatrix}
$$

$$
\boldsymbol{R}_{\text{CSL}} = \begin{pmatrix} 0.968 & -0.161 & 0.194 \\ 0.194 & 0.968 & -0.161 \\ -0.161 & 0.194 & 0.968 \end{pmatrix}
$$

which yields an average variation of 2.7° between the CSL and experimental case. From the Brandon criterion, this is within the limit for a CSL description.

5. Concluding remarks

A scheme has been described whereby microdiffraction data may be processed to produce accurate geometrical analyses of large numbers of grain boundaries in polycrystalline materials. On balance the stereographic manipulation procedure suggested by Ralph was considered to be optimal, despite the fact that the misorientation data are subsequently required in matrix form for comparison with high-density CSL cases. The justification for use of this stereographic method lies in its facility to self-check, and in its ease of application. The remaining steps necessary to compare experimental results with CSL theory have been described in some detail here. The program produces the required geometrical data with operator control only necessary for the initial choice of the high-density CSL which is closest in angular terms to the experimental boundary.

Acknowledgements

Financial support and supply of experimental material from the United Kingdom Atomic Energy Authority and the Generating Board is gratefully acknowledged. The authors would also like to thank Dr R. C. Ecob for many valuable discussions.

References

1. S. RANGANATHAN, *Acta Crystallogr.* **21** (1966) 197.
2. A. P. SUTTON, *Int. Met. Rev.* **29** (1984) 377.
3. H. GLEITER, *Mater. Sci. Eng.* **52** (1982) 91.
4. D. H. WARRINGTON, in "Grain boundary structure and kinetics" (ASM, Metals Park, Ohio, 1980) p. 1.
5. P. J. GOODHEW, in "Grain boundary structure and kinetics" (ASM, Metals Park, Ohio, 1980) p. 155.
6. R. W. BALLUFFI, in "Interfacial segregation", edited by W. C. Johnson and J. M. Blakely (ASM, Metals Park, Ohio, 1979) p. 193.
7. V. RANDLE and B. RALPH, in preparation.
8. C. T. YOUNG, J. H. STEELE and J. L. LYTTON, *Met. Trans.* **4** (1973) 2081.
9. C. GOUX, *Bull. cercle Études Métaux* **8** (1961) 185.
10. B. RALPH, PhD thesis, University of Cambridge (1964).
11. J. W. STEEDS, in "Introduction to analytical electron microscopy", edited by Hren, Goldstein and Joy (Plenum, New York, 1979) p. 387.
12. B. RALPH and R. C. ECOB, in Proceedings of 5th Risø International Symposium, Risø, September 1984, edited by Hessel Andersen, Eldrup, Hansen, Juul Jansen, Letters Lilholt, Pederson and Singh, p. 109.
13. J. W. EDINGTON, Monograph 2 in "Practical Electron Microscopy in Materials Science" (Philips Technical Library, Macmillan, 1975).
14. D. G. BRANDON, *Acta Metall.* **14** (1966) 1479.
15. D. H. WARRINGTON and M. BOON, *ibid.* **23** (1975) 599.
16. C. J. TWEED, PhD thesis, University of Cambridge (1983).
17. A. SANTORO and A. D. MIGHELL, *Acta Crystallogr.* **A29** (1975) 169.
18. P. H. PUMPHREY and R. M. BOWKETT, *Scripta Metall.* **6** (1972) 31.
19. V. RANDLE and B. RALPH, in Proceedings of EMAG 85, Newcastle upon Tyne, September 1985; International Conference Series No. 78 (Adam Hilger, Bristol) p. 59.
20. D. H. WARRINGTON and P. BUFALIN, *Scripta Metall.* **5** (1971) 771.

Received 18 November 1985
and accepted 10 January 1986